Revealing sphingolipids composition in extracellular vesicles and paternal *β*-cells after persistent hyperglycemia

Magdalena E. Skalska[a,b], Martyna Durak-Kozica[a,b] and Ewa Ł. Stępień[a,b*]

[a]*Department of Medical Physics, M. Smoluchowski Institute of Physics, Faculty of Physics, Astronomy and Applied Computer Science, Jagiellonian University in Krakow, Poland;*

[b]*Centre for Theranostics, Jagiellonian University, Kopernika 40 St, 31-501 Krakow, Poland.*

***Corresponding author:**

Ewa Ł. Stępień
Department of Medical Physics
M. Smoluchowski Institute of Physics
Faculty of Physics, Astronomy and Applied Computer Science
Łojasiewicza 11 Street
30-348 Kraków
e-mail: e.stepien@uj.edu.pl

Highlights

- ToF-SIMS effectively compares sphingolipid content in EVs and β-cells.
- Analysis shows profile variances in CER, HexCER, glycosphingolipids between EVs and parent cells.
- Hyperglycemia alters general glycosphingolipid content in cells and EVs per ToF-SIMS.

Abstract

Extended periods of hyperglycemia (HG) can lead to metabolic disorders of sphingolipids (SPs) and their subsequent accumulation in cells. This accumulation can trigger a range of complications, including kidney and neurodegenerative diseases. In our study, we compared the levels of selected ceramides (CER), hexosylceramides (HexCER), and glycosphingolipids (GSLs) in potential biomarkers - extracellular vesicles (EVs). These EVs were derived in vitro from human β-cells cultured under both normoglycemic and high-glucose conditions (HG). We utilized Time of Flight - Secondary Ion Mass Spectrometry (ToF-SIMS) for SP analysis. Our results confirmed that the lipid profiles of these three groups differ between large and small EVs, with some SP lipids being more enriched in EVs compared to cells. Interestingly, our study revealed that HG only regulates the lipid content from the glycosphingolipid group in relation to normoglycemia. Collectively, our findings underscore the potential applications of ToF-SIMS in characterizing the impact of different culture conditions on lipid levels. To the best of our knowledge, our study is the first to employ ToF-SIMS in analyzing the effects of HG on SP levels in EVs and their parental β-cells.

Keywords: ToF-SIMS, glycosphingolipids, extracellular vesicles, hyperglycemia, β-cells.

1. Introduction

Sphingolipids (SPs), including ceramides (CERs), hexosylceramides (HexCERs) and glycosphingolipids (GSLs), represent a ubiquitous and structurally miscellaneous class of lipids involved in physiological and pathological processes, possessing both signaling and structural properties [1,2]. Lipid membrane composition is varied in different cell compartments, and having impact on such cell membrane properties, charge and protein corona [3]. Hyperglycemia (HG) is an example of a physiological condition initiated by the elevated blood glucose levels, which, when out of control of the sensitive fuse that is the hormone insulin), causes metabolic stress, which, if it continues chronically, can cause pathological conditions. In fact in most of patients having glucose intolerance, HG goes silent early on and is often not detected until complications develop. What is known, however, is that the first stage in the development of complications is elevated glucose level for a dangerous period, followed by insulin resistance, eventually leading to type 2 diabetes mellitus (T2DM) [4]. An important role in glycemic control and HG prevention is played by pancreatic β-cells, which can compensate for high glucose concentrations by increasing insulin secretion [5]. This condition, in which HG is suppressed by insulin overproduction, can persist for years and may never develop into overt diabetes [6,7]. And yet, over time, the ability of β-cells to produce high levels of insulin may be diminished due to both abnormal cell signalling and increased apoptosis [8]. In this case, HG modifies the molecular composition of pancreatic β-cells that determine metabolic processes, accelerating the course of β-cells to failure and disease progression [9]. Indeed, SPs have been shown to actively participate in the HG-induced process, mediating the loss of insulin sensitivity, promoting the characteristic diabetic pro-inflammatory state, and inducing cell death and dysfunction of important organs such as the pancreas and heart [10,11]. However, given the high complexity of SP metabolism, it follows that its regulation may also be very complex or multifactorial.

Time of Flight – Secondary Ion Mass Spectrometry is an example of an advanced physical method adapted to metabolomics and lipidomic research. This technique has been successfully used for the characterization of lipids in biological samples and comparative analyzes of cells, tissues, organs and even organisms [12–14]. In this study, we would like to focus on SPs composition in β-cells and their residues and metabolites secreted in the form of extracellular vesicles (EVs) using ToF-SIMS.

EVs are spherical nanostructures surrounded by a lipid bilayer ranging in size from 30 to 1000 nm. EVs can be divided into several subpopulations that differ in biogenesis, size, cargo

and function [15]. Currently, the main EV populations recognize large EVs (150 – 1000 nm) and small EVs (50 – 150 nm) [16]. Their size is of great importance because it can be used to assume the biogenesis and function of EVs, while large EVs are directly secreted from the cell membrane, small EVs accumulate in the lumen of late endosomal compartments and are released into the extracellular space after endosome fusion with the cell membrane [17,18].

It is believed that the most important function of EVs is the transfer of intercellular information in the form of nucleic acids (miRNA), proteins and lipids. They contain characteristic cell-derived molecules that reflect the intercellular status of their parent cell. Thanks to this cargo, they affect the physiological and pathological reactions of cells receiving the transmitted data, thus taking an active part in maintaining the homeostasis of the biological system by transmitting information, but also expelling unnecessary material [19]. Research results of the last decade have revealed that EVs are released from various cells, and their cargo is involved in various disorders, mainly cancer, neurological and metabolic, e.g. diabetes [20]. In biomarker studies but also to understand EV signalling properties, the molecular characterization of EVs obtained from different cellular models (cell cultures) is essential in both basic and preclinical research [16,21–23].

The lipid composition of EVs is reflective of the cells from which they originate [24]. Consequently, it can be inferred that the composition of sphingolipids (SPs) in EVs would vary based on the cell culture they are derived from, as well as the conditions under which they were cultured. Past studies have indicated that the molecular composition of both cells and EVs can be altered by external culture conditions [25]. However, it remains to be seen whether an elevated glucose concentration in the external environment can modify the profile of ceramides (CERs), hexosylceramides (HexCERs), and glycosphingolipids (GSLs) in the composition of β-cell membranes and EVs.

In this study, we employ ToF-SIMS mass spectrometry to compare the profiles of selected sphingolipids (CER, HexCER and GSL) in EVs samples derived from a β-cell line with the compositions cells cultured under HG conditions.

2. Materials and methods

2.1. Cell cultures

The insulin-releasing pancreatic β-cell line (1.1B4, Merck KGaA, Sigma Aldrich, Darmstadt, Germany) was cultured in a 175 cm^2 cell culture bottles and maintained in RPMI 1640 medium (cat. No. 11879020 Gibco for normoglycemia and hyperglycemia, 21875158 Gibco for medium hyperglycemia), supplemented with 10% Fetal Bovine Serum (FBS; cat. No. 16000036, Thermo Fisher Scientific, Waltham, MA, USA), 2 mM L-glutamine (cat. No. G7513 Sigma-Aldrich, Darmstadt, Germany) and antibiotics - 100 µg/ml streptomycin with 100 units/ml penicillin (cat. No. 15140122 from Sigma-Aldrich, Darmstadt, Germany). Cells were grown as monolayers in an incubator under conditions of a humidified 5% CO_2 atmosphere and 37 °C until they reached about 80% confluence. The culture was maintained by changing the medium and passaged with trypsin (Trypsin-EDTA solution, cat. No. 25200056 Thermo Fisher Scientific, Waltham, MA, USA). The first part of the bottles were grown in a medium containing 5 mM D-glucose (cat. No. G8270 Sigma-Aldrich, Darmstadt, Germany) to obtain normoglycemic control (NG), the second part was cultured under long-term, containing 3 passages, medium hyperglycemia conditions - MDM (11 mM D-glucose), while the last, third part of cells were grown in the highest concentration of glucose to obtain hyperglycemia (25 mM D-glucose) conditions - HG. The next key step was to starve cells for 24 hours by changing the medium to a serum-free medium (without FBS). Finally, after the fasting period, culture bottles were shaken mechanically, and the medium was collected for subsequent centrifugation and low-pressure filtration dialysis to concentrate and isolate EVs. The medium was collected from 12 culture bottles for all culture conditions. From each 4 cell culture bottles, the medium was collected in a separate container (approximately 120 ml), which made it possible to obtain 3 biological replicates for NG, MDM and HG conditions.

2.2. Cells Harvesting

For the purpose of comparing the molecular composition of lipids, cells were collected after the serum starvation period in NG, MDM and HG by trypsinization. Cells were suspended in PBS and then frozen at -80 °C for simultaneous analysis with isolated EVs.

2.3. EVs Isolation

Collected volumes of β-cell conditioned medium were first subjected to two preparatory centrifugations to remove intact cells, cell debris and apoptotic bodies (**Fig. 1**). Cell media samples were successively centrifuged at 400 x *g* (10 min) and 3,000 x *g* (25 min),

both at 4 °C. Subsequently, each 120 ml sample was filtered under Low-Pressure Filtration Dialysis (L-PFD) using a cellulose dialysis membrane (cat. No. 131486, Spectra/Por Biotech) with a molecular weight cut-off (MWCO) of 1000 kDa (width: 16 mm, diameter 10 mm). To accelerate the filtration process, a reduced pressure of -0.2 bar was applied in the system, which was used to obtain the final sample volume of about 1.5 ml [26,27]. The membrane was then washed with 10 ml of deionized water.

The resulting EV suspension was subjected to a differential centrifugation process. In the first step, samples were centrifuged for 30 min at 7,000 x *g* at 4 °C and 18,000 x *g* for 20 min to **pellet large EVs**. The resulting supernatant was transferred to 1.5 ml top-opening centrifuge tubes and centrifuged for 1.5 h at 150,000 x *g* at 4 °C (Sorvall MX 150+ Micro-Ultrawiring, Thermo Fisher Scientific, Waltham, MA, USA) to obtain **small EVs subpopulation**.

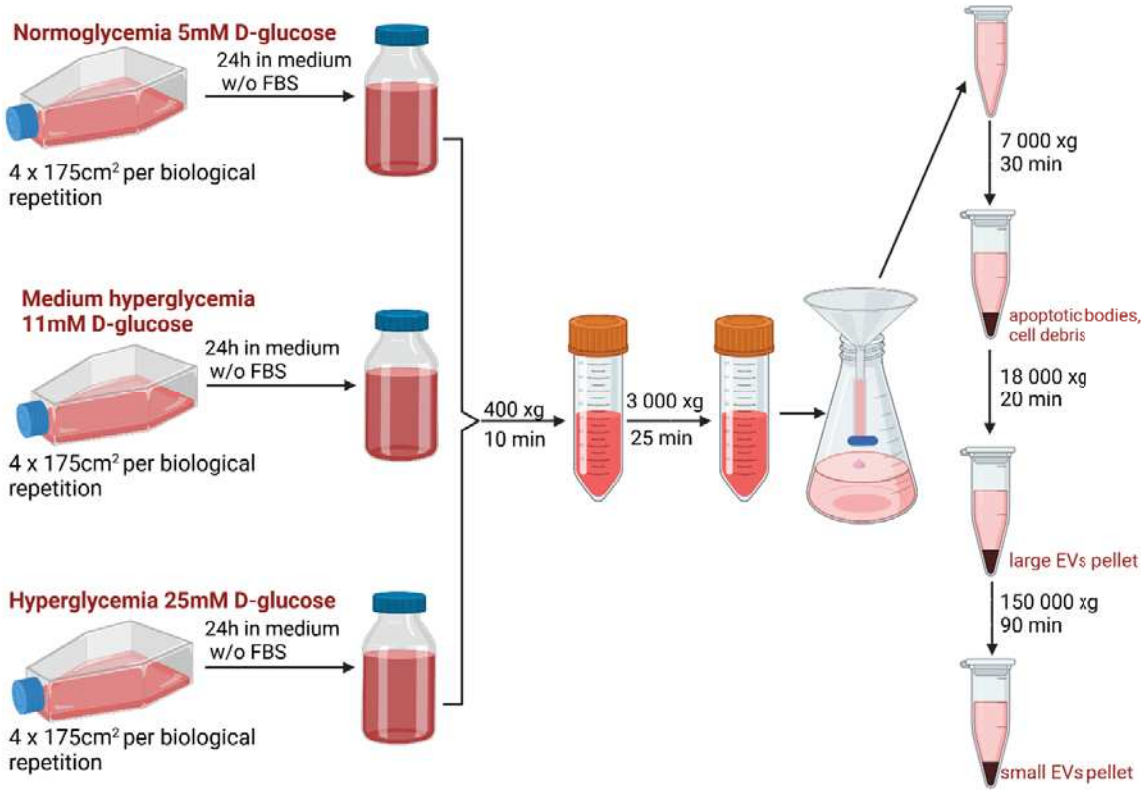

Fig. 1. *Scheme of the extracellular vesicle isolation procedure.*

Pellets were resuspended in 50 µl PBS (cat. No. 10010023 Thermo Fisher Scientific, Waltham, MA, USA) in triplicate and stored at -80 °C for further characterization and ToF-SIMS analysis.

2.4. Antibodies for flow cytometry measurement

The following labels were used to characterize small and large EVs samples: FITC Annexin V (BioLegend, cat. 640906) and antibodies Alexa Fluor 700 anti-human CD63 (BioLegend, cat. 353024), APC anti-human CD81 (BioLegend, cat. 349510) and PE anti-human CD9 (BioLegend, cat. 312106).

2.5. Spectral Flow Cytometry

Both small and large EVs, isolated from 120 mL of conditioned media per sample (divided into 4 groups) were incubated with Annexin V and antibodies against CD63, CD9 and CD81 for 45 min on ice. EVs samples were analysed using the ID7000 apparatus (spectral flow cytometer, SONY), a sample volume was set to 100 µL. Prior to analysis, the Sony ID7000 was calibrated using alignment checks (Sony Biotechnology Inc AlignCheck Flow Cytometer Alignment Beads 107/mL 10 µm, 2 mL, cat. no AE700510) and the 8□peak performance beads (Sony Biotechnology Inc 8 Peak Bead cat. no AE700522, 107/mL 3.1 µm, 5 mL cat. no AE700510), according to the instrument supplier's guidelines.

2.6. Transmission Electron Cryomicroscopy (cryo TEM)

About 3□µL of the sample solution was applied on freshly glow-discharged TEM grids (Quantifoil R2/1, Cu, mesh 200) and plunge-frozen in liquid ethane using the Vitrobot Mark IV (Thermo Fisher Scientific). The following parameters were set: humidity 95%, temperature 4□°C, blot time 2□s. Frozen grids were kept in liquid nitrogen until cut and loaded into the microscope. Cryo-EM data were collected at the National Cryo-EM Centre SOLARIS (Kraków, Poland). Movies (40 frames each) were gathered using the Glacios microscope (Thermo Fisher Scientific) with 200□kV accelerating voltage, 190 kx magnification and corresponding to the pixel size of 0.74□Å/px. The direct electron detector Falcon4 was used to obtain data, operated in counting mode. Imaginate areas were exposed to 40 e-/Å2 total dose each (measured *'on vacuum'*). Images were acquired at under-focus optical conditions.

2.7. Transmission Electron Microscopy (TEM)

For negative staining, a copper grid coated with formvar and carbon was used. Samples were incubated for 3 min on grids. After this time, the excess was drained with a piece of filter paper. Next, grids were washed on two drops of distilled water and uranyl acetate. After

rinsing grids were left on a drop of uranyl acetate for 1min, and then dried in the air. For observation, the JEOL JEM 2100HT electron microscope (Jeol Ltd, Tokyo, Japan) was used at 80 kV accelerating voltage. Images were taken using a 4kx4k camera (TVIPS) equipped with EMMENU software *ver*. 4.0.9.87. The image analysis was performed using the Fiji program. The histogram was made based on 100 EVs counts.

2.8. ToF-SIMS analysis

Time of Flight - Secondary Ion Mass Spectrometry (ToF-SIMS) is an analytical surface technique based on bombarding the examined surface with a pulsating beam of ionized atoms (single atoms or clusters). In the case of biological samples, ionized clusters of bismuth or fullerene (Bi_3^+, C_{60}^+) are most often used, which allow the detection of larger molecules by minimizing damage to the structure being tested. The spectrometer uses a time-of-flight analyzer with high mass resolution (up to $m/\Delta m$ = 10,000) and high transmission, in which the time of flight of emitted secondary ions through a vacuum tube is measured, these are ionized whole biomolecules, ionized fragments of these biomolecules or newly formed ionized conjugates. Some of these ionized molecules are characteristic fragments of biomolecules that are components of the tested biological structure, e.g. amino acids, lipids or metabolites, enabling the qualitative characterization of the sample surface [28].

The described analysis is possible in the so-called *static mode*, in which the dose density threshold of primary ions deposited on the tested surface is valid. The measurement in this range ensures that the surface will not be damaged, and the components will not be significantly delocalized and fragmented in the sample volume. At the same time, the ToF-SIMS enables imaging of 2D maps of secondary ions emission from the surface with a submicron spatial resolution (*dynamic mode*), this is the second operating mode of the spectrometer with reduced mass resolution [29].

A significant advantage of the ToF-SIMS technique in relation to biological samples is its ability to perform comparative analyses of experimental samples with control samples. This is done by assessing the intensity of peaks characteristic of the biomolecules of interest, eliminating the need to extract these compounds from the biological structure or to label these structures in the sample. This feature is particularly important for lipids that are susceptible to oxidative processes. However, the requirement of high vacuum measurement in an analytical chamber poses a challenge for biological research, adding a layer of complexity to the procedure of preparing biological samples.

2.9. Sample preparation and ToF-SIMS measurement parameters

For ToF-SIMS measurements, silicon wafers (cat. No. 647780, Sigma Aldrich, St. Louis, MO, USA) with dimensions of 1 x 1 cm^2 were prepared. The selection of the silicon substrate was dictated by previous studies examining the best parameters for ToF-SIMS studies on biomaterials [30]. Before EVs and cells deposition, each substrate was sonicated in toluene (cat. No. 244511, Sigma Aldrich) and ethanol (absolute, 99%, cat. No. 396480111, POCH) for 10 min using an ultrasonic bath, rinsed with plenty of deionized water, and then dried with N_2. For each experimental group, two samples deposited on the silicon surface with a volume of 30 µl were prepared.

To obtain all spectra, the ToF-SIMS 5 instrument (ION-ToF GmbH, Münster, Germany) was used with a Bi_3^+ liquid metal ion gun (30 keV) as the primary ion source. Data were recorded in the mass range up to 900 Da with a mass resolution of 8,300 at *m/z* 600 (FWHM) and an analysis surface size of 150 × 150 μm^2 for positive ions (125 x 125 pixels) in three locations on one sample. During all experiments, the residual gas pressure in the spectrometer chamber was maintained at 10^{-7} mbar. The lipid composition analysis was performed in the static spectrometer mode with a current equal to 1.10 pA. A low-energy electron gun was used in the interval between two pulses from the primary ion source to neutralize the charge formed on the sample surface during the bombardment. Measurements were carried out simultaneously and under the same conditions using a single sample holder, allowing for comparative data analysis. Each spectrum was calibrated using signals for positive ions: H^+, H_2^+, CH^+, CH_2^+, CH_3^+ and $C_3H_2^+$.

2.10. Statistical analysis

In the ToF-SIMS technique, there is a matrix effect exists that complicates the acquisition of quantitative information. However, it is still feasible to obtain semi-quantitative information through the appropriate preparation of measured data, such as spectra normalization and selection of regions of interest [31]. The normalization of raw ToF-SIMS data is typically performed to mitigate artifacts induced by topographic, apparatus, or matrix effects [32]. This can be accomplished in several ways. In this study, we normalized each

spectrum to the total dose deposited on the examined surface, a step that eliminates the impact of differences arising from the compiled beam of primary ions [33].

Fig. 2 presents the workflow of the process of preparing data from spectra for comparative analysis. From each of the sixteen surface measurements of 150 x 150 μm^2 (nine sample types, two areas of 50 x 50 μm^2 were selected for each sample type (tour biological replicates for each group and four 150 x 150 μm^2 measurements on the one sample).

The selection of a smaller *Region Of Interest* (ROI) was preceded by the examination of 2D emission maps for ions characteristic of the analysed SP fragments, which helped to eliminate local artifacts. For each experimental group (NG, MDM and HG cells, NG, MDM and HG large EVs, NG, MDM and HG small EVs), 32 mass spectra from 50 x 50 μm^2 regions were included in the comparative analysis. The spectra thus obtained were further analyzed, which included the identification of characteristic lipid peaks such as protonated ions, adducts, and pseudo-molecular ions.

The peaks included in the analysis correspond to the masses characteristic of specific chemical structures. It should be noted that different molecular formulas may correspond to the same molecular weight. Only peaks with a high likelihood of matching the structures of interest and those that have been previously described and used in the ToF-SIMS analyses were included in the comparative analysis.

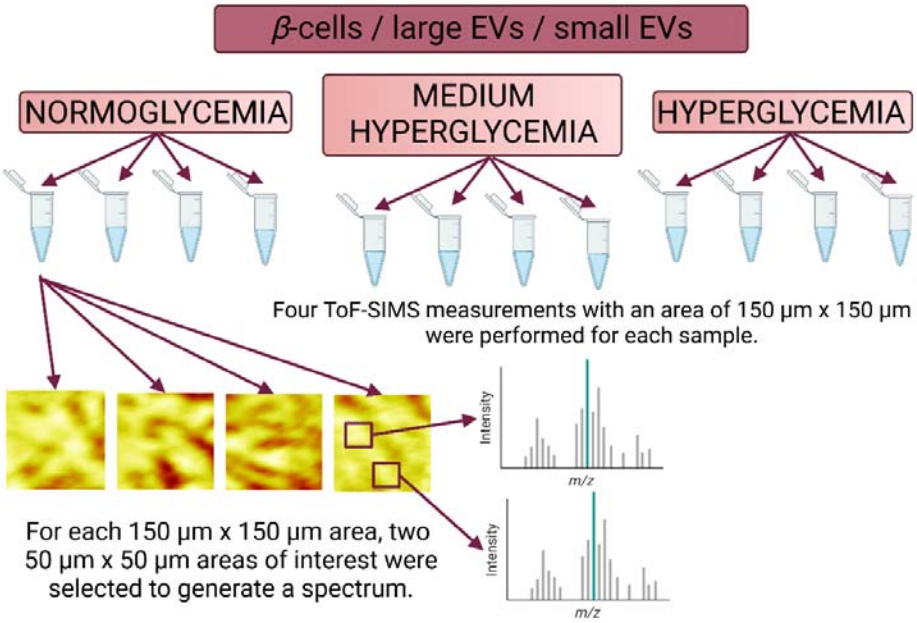

Fig. 2. *Workflow of obtaining spectra for comparative analysis.*

The obtained intensity of the selected peak, i.e. the integrated area under the characteristic peak curve, was normalized to total counts for a given spectrum in the area of 50 × 50 μm^2. Statistical analysis was performed, in which mean values and intensity standard deviations were calculated for selected peaks for each group of samples. The SurfaceLab software (*ver*. 7.2) was used to analyze the data, enabling re-editing of the measurements taken and the academic version of OriginPro (*ver*. 9.8.0.200, 2020b) was used.

3. Results

3.1. Spectral Flow Cytometry

In order to identify the types of EVs present in our isolated samples, we conducted a flow cytometry analysis. Annexin-V was utilized as a marker for ectosomes, and we detected an annexin-V-positive signal in both small and large EV samples. We also used CD9, CD63, and CD81 as markers for exosomes (as well as for small ectosomes), and detected positive signals in both samples. Notably, the expression of annexin-V and CD9 was higher in large EVs, while CD63 and CD81 were more prevalent in the population of small EVs. As demonstrated, pure PBS yielded only a minimal signal (**Fig. 3**).

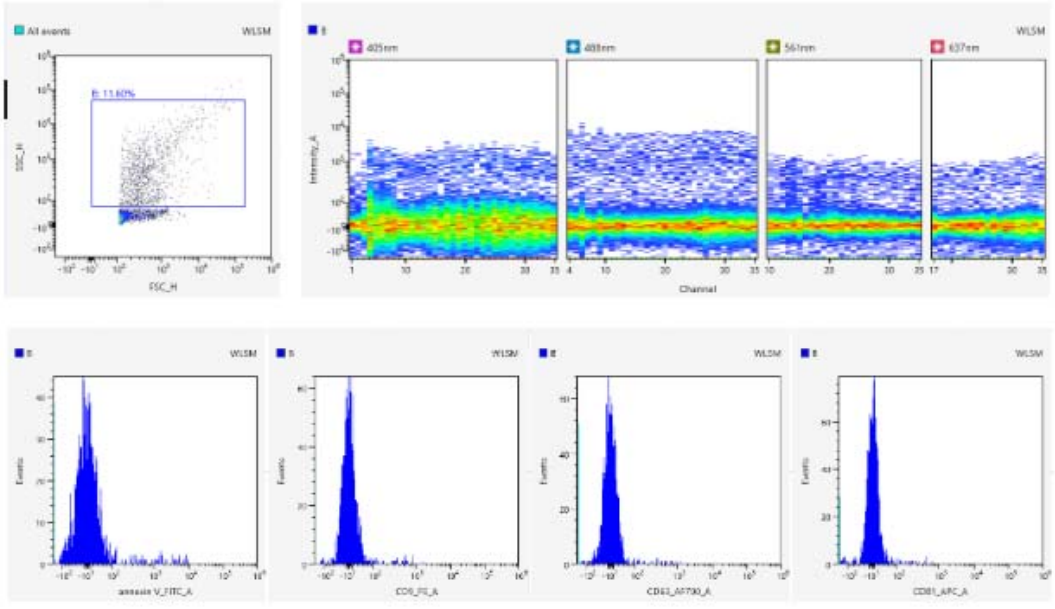

Fig. 3. *The results of the ID7000 spectral flow cytometry analysis for pure PBS.*

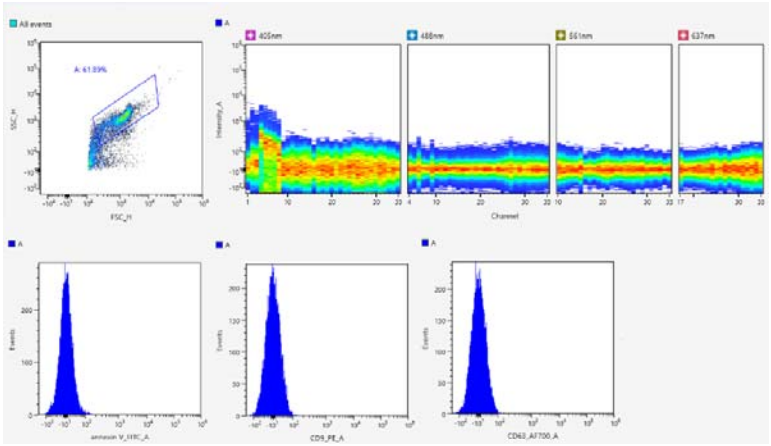

Fig. 4. *Unstained ectosomes analysis on ID7000 flow cytometry.*

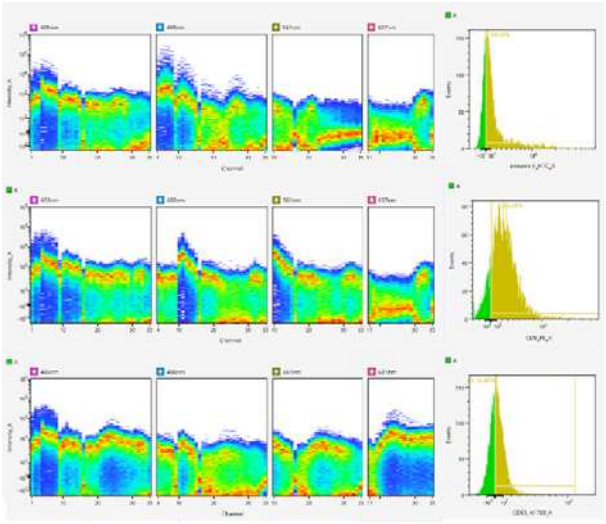

Fig. 5. *Single and quadruple dyed ectosomes analysis on ID7000 flow cytometry.*

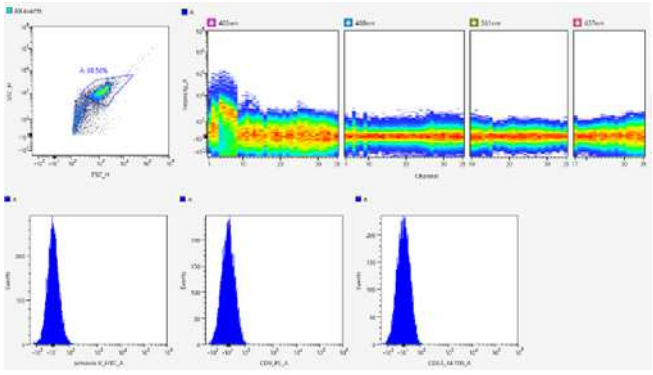

Fig. 6. *Unstained exosomes analysis on ID7000 flow cytometry.*

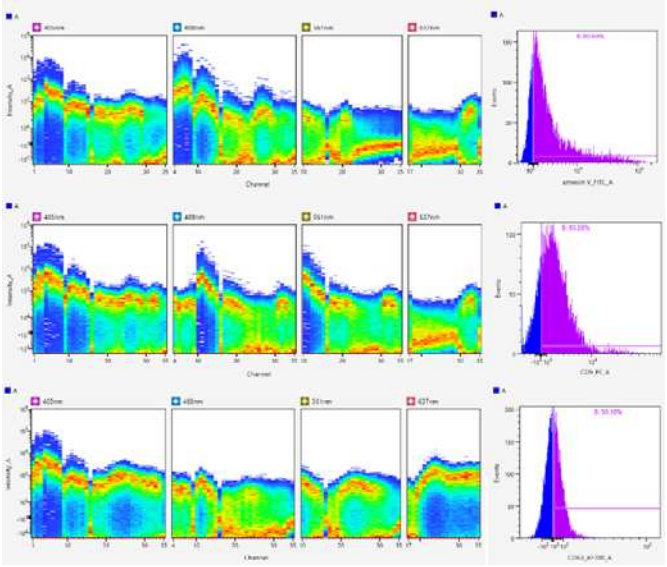

Fig. 7. *Single and quadruple dyed exosomes analysis on ID7000 flow cytometry.*

3.2. TEM

The images in **Fig. 8** depict an unoccupied copper grid, thereby validating the effective isolation of EVs. The large EVs exhibit an average size of approximately 150 nm, while the small EVs demonstrate a mean size of about 60 nm. The findings obtained through TEM microscopy not only confirm the distinct sizes and shapes of both EV populations but also indicate a higher concentration of small EVs.

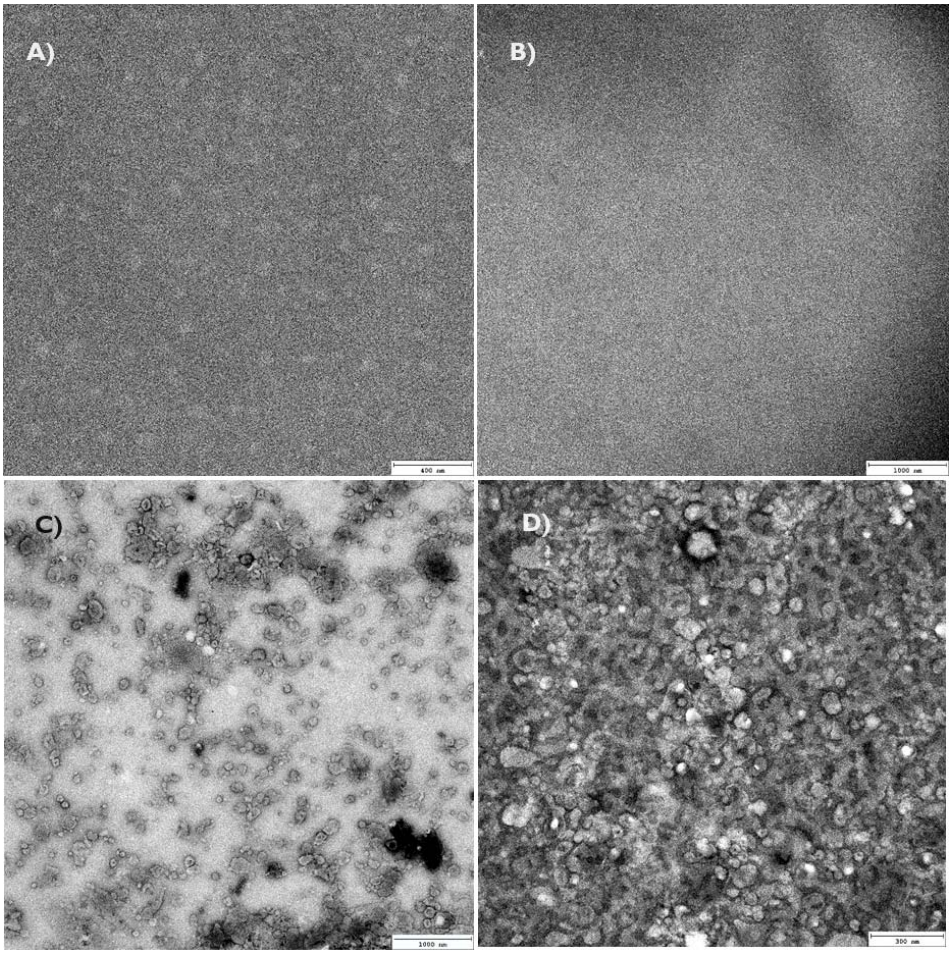

Fig. 8. *The copper grid A) before contrasting, B) after contrasting, C) the population of large EVs, and D) the population of small EVs.*

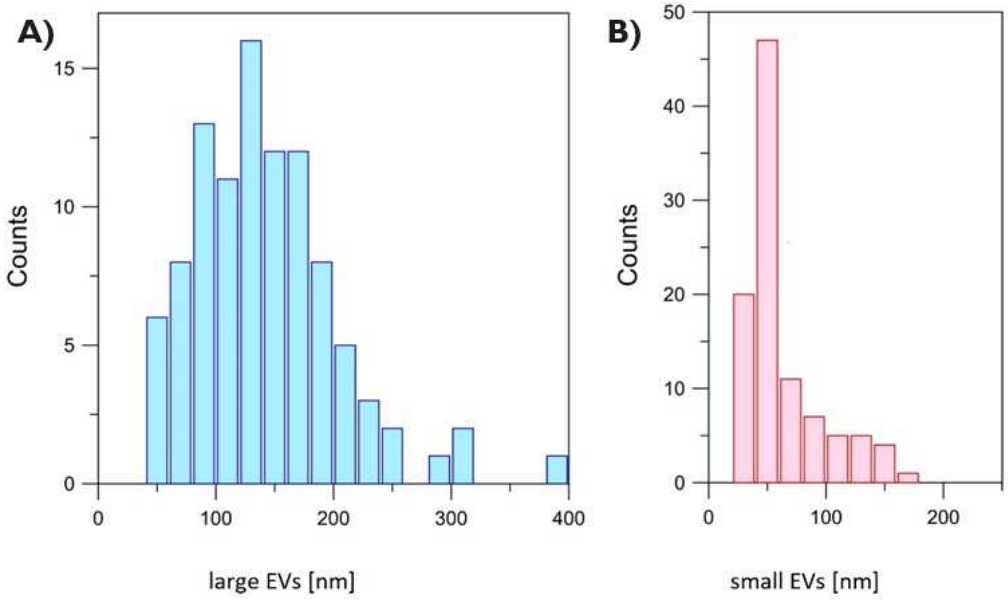

Fig. 9. *The size distribution for A) large and B) small EVs.*

3.3. CryoTEM

Images captured using CryoTEM microscopy reveal the double membrane encapsulating the EVs, as well as the cargo inside the vesicle. In the example of large EVs (as shown in **Fig. 9**), the crown-like structure can be observed on their surface. TEM and CryoTEM studies have confirmed the absence of cells, cellular organelles, or any other cellular debris in the EV samples.

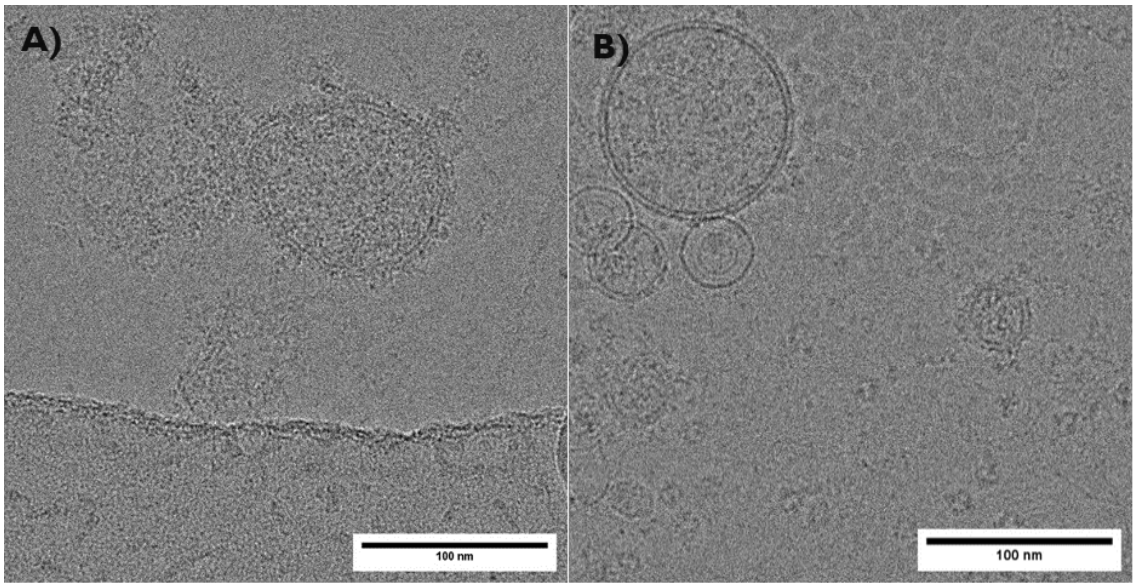

Fig. 9. *The CryoTEM image of A) large EVS, and B) small EVs*.

3.4. ToF-SIMS analysis

The molecular composition of EVs is believed to reflect the composition of secretory cells in their proportions and is also modified in parallel by various factors [34]. Thanks to their structure, but also the contained cargo, EVs transfer information to other biostructures [35]. This information is encoded in the presence and quantity of building blocks, including approximately 9,769 proteins, 1,116 lipids, 3,408 mRNAs and 2,838 miRNAs, illustrating their complexity and potential functional diversity [36]. In this analysis, attention was paid to three characteristic groups of lipids: ceramides (CERs), hexosylceramides (HexCERs) and glycosphingolipids (GSLs).

The lipids chosed for analysis form part of the cellular endosomal complex that orchestrates and directs the endogenesis pathway within the cellular system. As such, they represent a crucial group of compounds that influence the formation of membrane-like

structures secreted by cells, mainly CERs and other SPs [37]. Importantly, they impact the content and destination of the endosome [38–40]. The dominant CERs in small EVs are C18:0-Cer and C24:1-Cer molecules, which enable the membrane folding, facilitating the budding of internal vesicles, but at the same time participate in the differentiation of secreted small EVs [41]. GSLs also exist in the form of lipid rafts (lipid microdomains), which can manifest as a lipid region enveloping and penetrating the surface membrane or as a flat lipid raft. These structures are enriched with specific types of lipids, such as sterols, SPs, and glycosylphosphatidylinositols. Through structural changes in lipid raft components and protein sorting and the formation of complexes with tetraspanins or flotillins, they play a pivotal role in endosomal biogenesis [42,43].

Numerous prior studies have indicated that SPs play a role in the progression of various pathologies, including obesity and type 2 diabetes mellitus (T2DM) [44]. Therefore, recognizing positive or negative correlations between SP levels and outcome conditions may contribute to the identification of useful and early biomarkers of these pathologies.

For the aforementioned lipid classes, the ToF-SIMS technique was used to check the changes in the normalized, average intensity of characteristic peaks changes in the case of β-cells, large and small EVs secreted by these cells.

a) Ceramides (CERs)

CERs consist of a long-chain or sphingoid base linked to fatty acids by amide bonds. Free CERs are present in membranes in small amounts, they perform specialized regulatory functions in cellular metabolism, often depending on the chain length of their fatty acyl components. Particular attention was paid to CERs and their functions in the regulation of apoptosis as well as cell differentiation, transformation and proliferation [45].

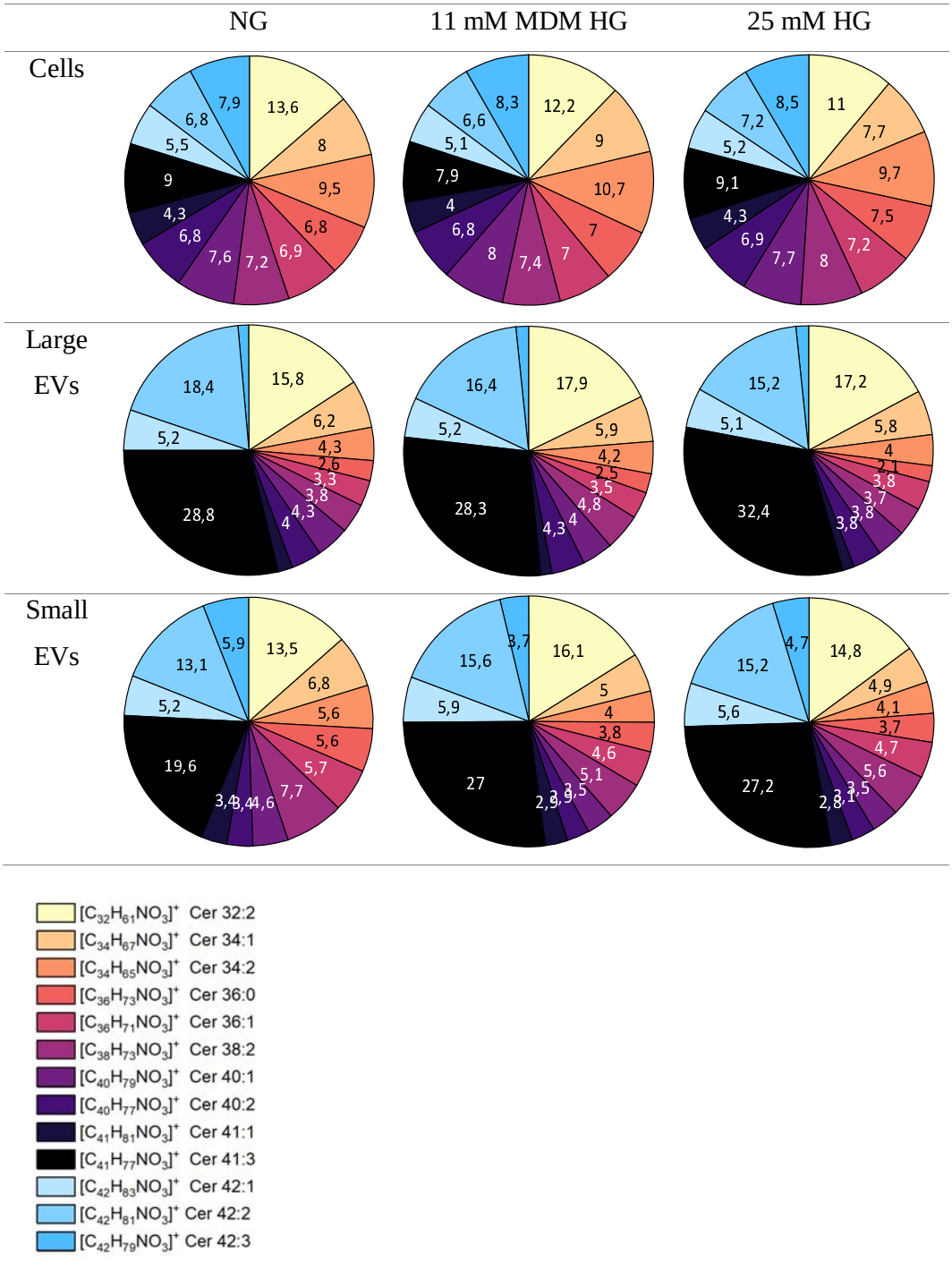

Fig. 10. *Comparison of percentages calculated from the mean, normalized ion intensities of characteristic peaks in positive polarity for ceramides (CER) in the case of normoglycemia (NG), moderate hyperglycemia (11 mM MDM HG) and hyperglycemia (25 mM HG).*

The circular charts presented in **Fig. 10** compare all types of samples taken for analysis. There are several dependencies for 13 masses characteristic of the CER group. First of all, it is worth looking at the changes resulting from different breeding conditions, and thus the impact of hyperglycemia on CER levels. Analyzing the relative values occurring to cells in the case of glucose concentrations, it is visible that the change in breeding conditions did not significantly affect the changes in the content of CER lipids. The only noticeable differences apply to NG and HG in the case of $[C_{32}H_{61}NO_3]^+$ - Cer 32:2 (*m/z* 508,72), for which in HG conditions relative content decreased by 2.6%. For other characteristic masses, the changes are less than 1%. The intensity values for the mentioned mass also differed in the case of large and small EVs, for which HG caused an increase in the content of this CER. In the case of large EVs, differences were also demonstrated for $[C_{41}H_{77}NO_3]^+$ - Cer 41:3, the content of which decreased with the increased glucose level, and for $[C_{42}H_{81}NO_3]^+$ Cer 42:2, for which the content increased. For small EVs, the largest differences were observed for $[C_{42}H_{81}NO_3]^+$ - Cer 42:2, for which, as in large EVs, the content increased significantly, for other characteristic ions, differences of up to 2% were observed.

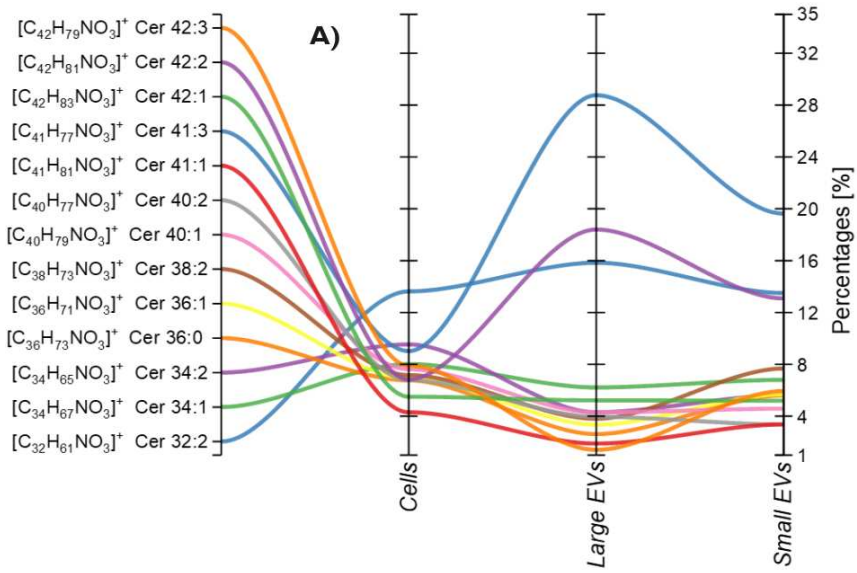

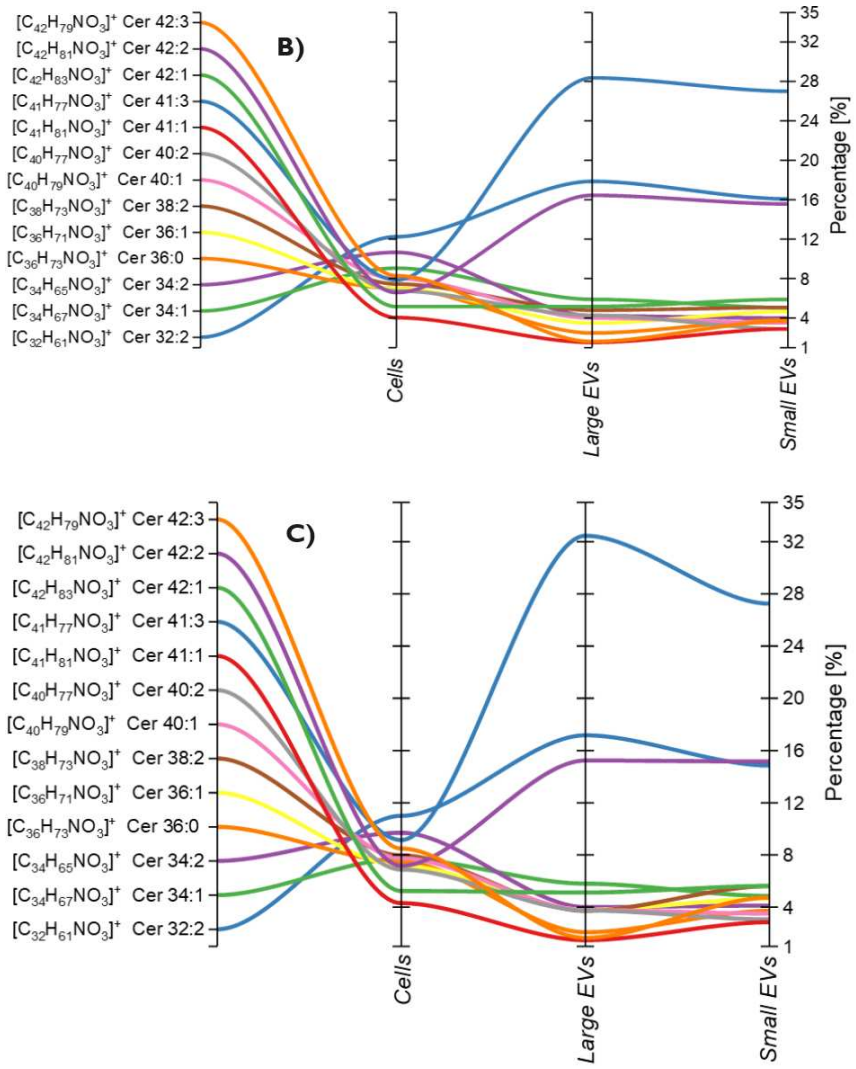

Fig. 11. *Percentage content changes in the case of the CER group for A) normoglycemic (NG) cells (5 mM D-glucose), B) moderately glycemic cells (11 mM glucose), C) hyperglycemic cells (25 mM D-glucose).*

The charts in **Fig. 11** illustrate changes in the CER group content between cells, large and small EVs. **Fig. 11** shows that large and small EVs have been significantly enriched in $[C_{34}H_{67}NO_3]^+$ - Cer 34:1, $[C_{36}H_{73}NO_3]^+$ - Cer 36:0 and $[C_{42}H_{79}NO_3]^+$ - Cer 42:3 compared to the cells from which they were isolated. In the case of the remaining masses characteristic of the CER group, the changes are within 4%. A similar trend was observed for the other two cultured conditions.

a) Hexosylceramides (HexCER)

HexCER consists of a ceramide backbone (a long-chain base connected to a fatty acid by an amide bond) linked to a neutral sugar molecule. The fatty acid and the long chain base can be of different lengths, be hydroxylated and contain double bonds. Due to the different combination of both components, a large number of monohexosylceramides can be distinguished, for example, 56 of them have been isolated from human plasma, which gives a greater variety in terms of CER, but a much smaller amount [46,47]. They are usually key precursors for the biosynthesis of more complex glycosphingolipids (including globosides and gangliosides), but they are also structural components of cell membranes and lipid rafts [48].

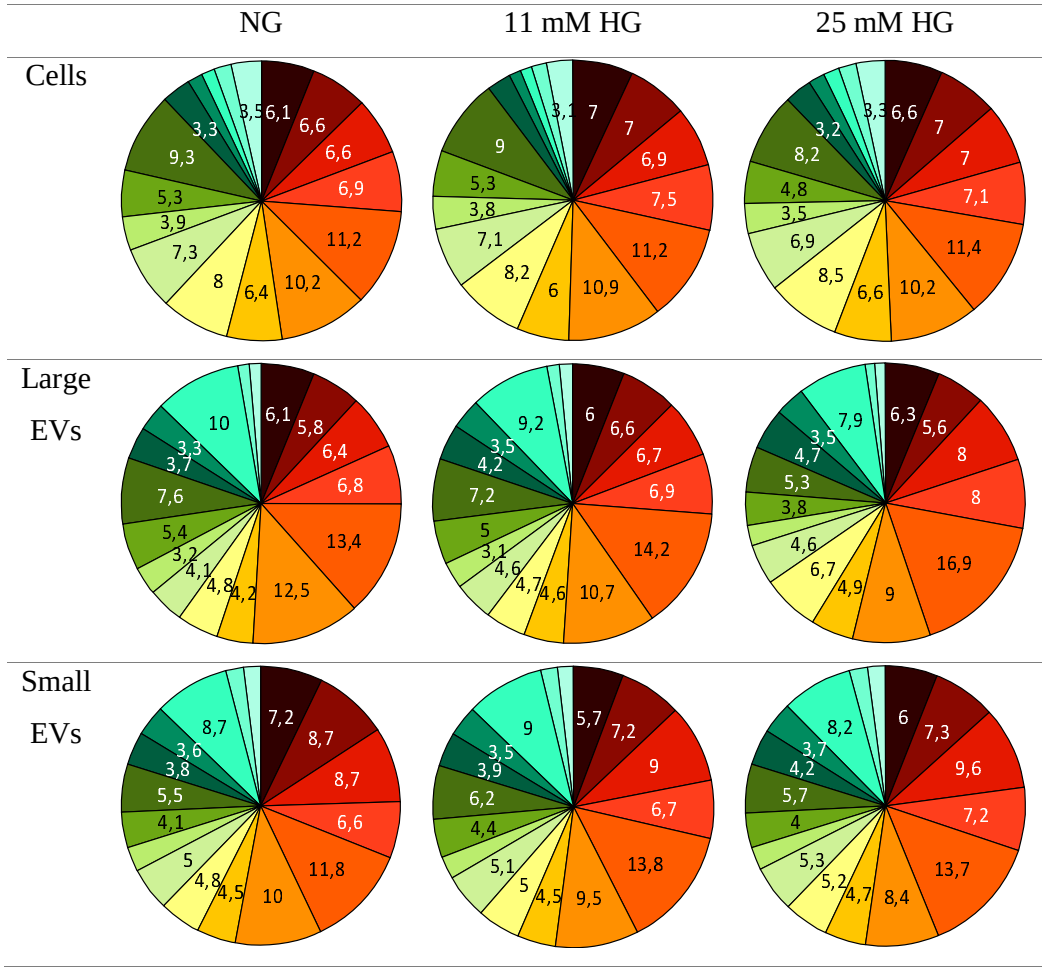

Fig. 12. *Comparison of percentages calculated from the mean, normalized ion intensities of characteristic peaks in the positive polarity of hexceramides (hexCER) in normoglycemia (NG), moderate hyperglycemia (11 mM MGM) and hyperglycemia (25 mM HG).*

As seen in **Fig. 12**, the analysis performed did not show any changes caused by hyperglycemic conditions in the β-cell culture. In the case of large and small EVs, a slight increase in the content of $[C_{42}H_{83}NO_8]^+$ HexCer 36:0, $[C_{42}H_{81}NO_8]^+$ HexCer 36:1 is visible, with a simultaneous decrease in the content of $[C_{42}H_{79}NO_8]^+$ HexCer 36:2.

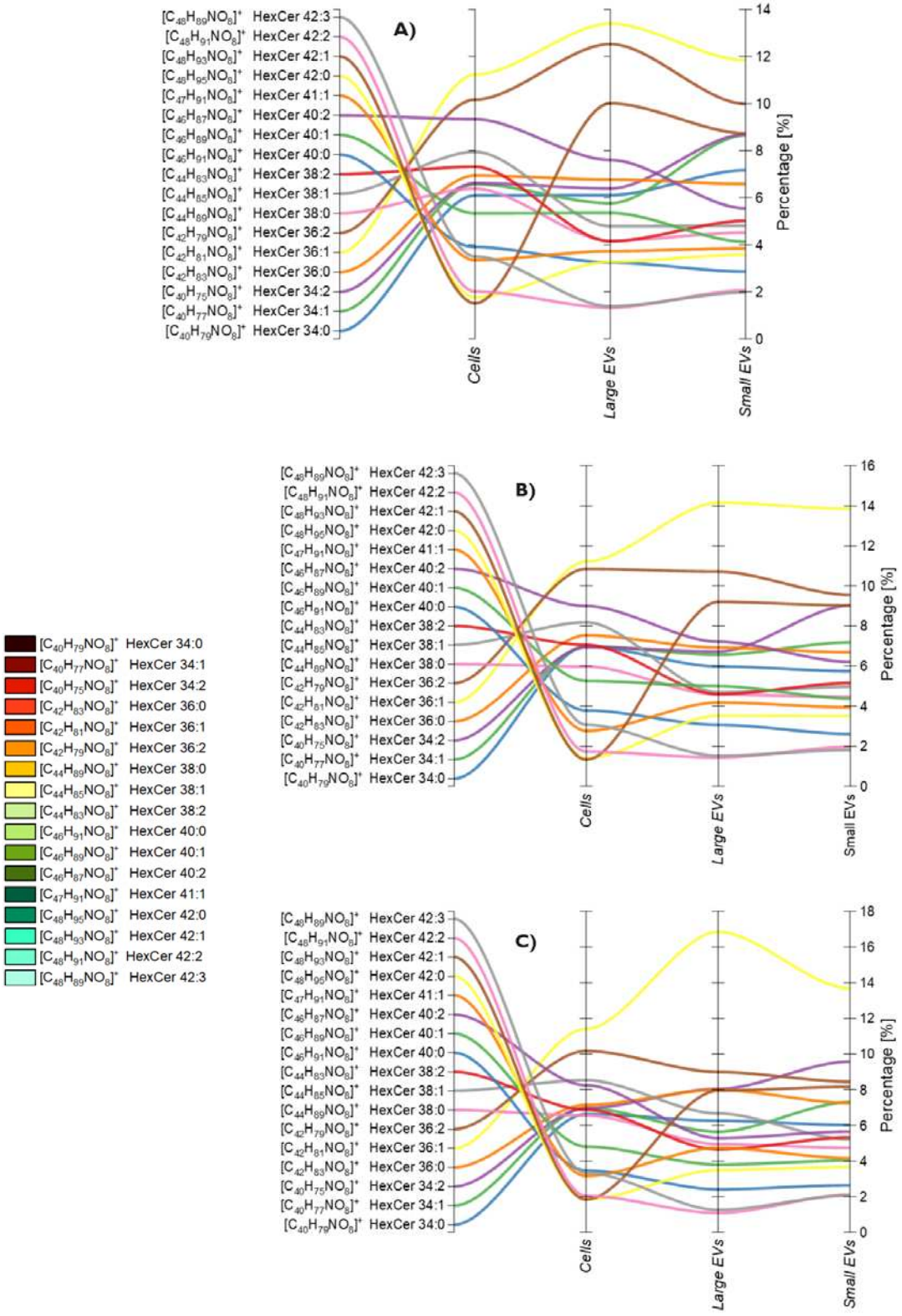

Fig. 13. *Percentage content changes in the case of the hexCER group for A) normoglycemic cells (5 mM D-glucose), B) moderately glycemic cells (11 mM glucose), C) hyperglycemic cells (25 mM D-glucose).*

17 peaks characteristic of hexCER with different acid lengths and different numbers of double bonds (0-2) were analyzed. The analysis revealed several differences recurrent for all three culture conditions when comparing cells, large and small EVs. A decrease in the content in all EVs samples in relation to cells was observed for: $[C_{44}H_{89}NO_8]^+$ HexCer 38:0 (*m/z* 760.62), $[C_{44}H_{85}NO_8]^+$ HexCer 38:1 (*m/z* 756.60), $[C_{44}H_{83}NO_8]^+$ HexCer 38:2 (*m/z* 754.54), $[C_{46}H_{87}NO_8]^+$ HexCer 40:2 (*m/z* 782.60), with a simultaneous increase for $[C_{48}H_{93}NO_8]^+$ HexCer 42:1 (*m/z* 812.62) and $[C_{42}H_{81}NO_8]^+$ HexCer 36:1 (*m/z* 728.51). The content of the remaining lipids from the hexCER group changes insignificantly by approximately 1% or is at the same level.

b) Glycosphingolipids (GSLs)

GSLs consist of a hydrophilic carbohydrate chain and a hydrophobic ceramide. The carbohydrate chain often acts as a ligand for carbohydrate-recognizing molecules, while the ceramide moiety forms an anchoring domain in the outer part of the cell membrane [49–51]. The region formed by the ceramide part allows membrane proteins to function as receptors, channels and transporters. The involvement of GSLs in microdomain formation is critical due to their ability to form systems through hydrogen bonds by donor and acceptor functional groups in ceramides and because of the hydrophobic interactions between their long-saturated acyl chains. GSLs are also found in membrane rafts containing detergent-insoluble membrane components and signalling molecules [52,53]. Moreover, GSL is a group of compounds that differ in composition, quantity and distribution across species, tissues, and cells. In cells, this type of compounds most often occurs as an integral component of cell membranes, especially extracellular surface membranes.

GSLs are involved in a variety of physiological functions. It has also been shown that GSLs are involved in the processes that create inflammation, including cancer, Alzheimer's disease, and others. Therefore, it seems justified to discover additional information about this group of compounds [54–58].

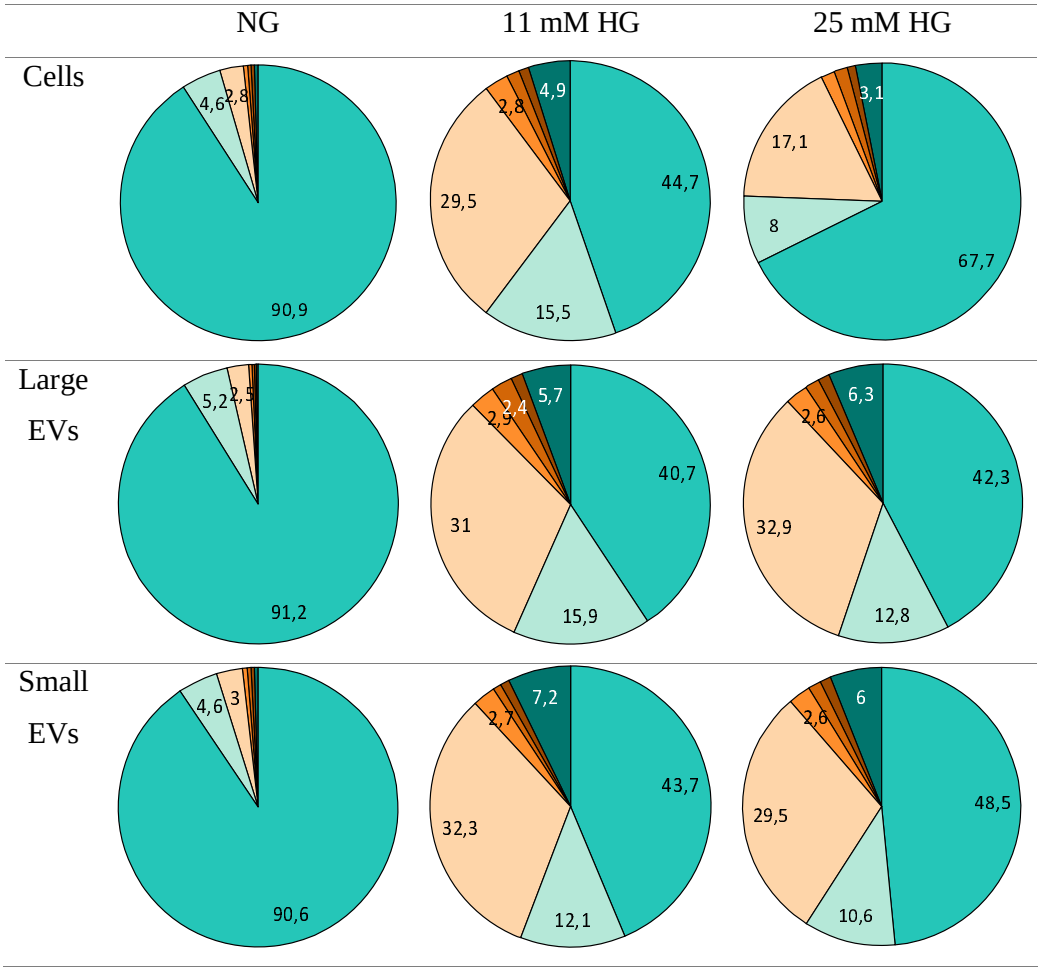

Fig. 14. *Comparison of percentages calculated from the mean, normalized ion intensities of characteristic peaks in the positive polarity of glycosphingolipids (GSLs) in normoglycemia (NG), moderate hyperglycemia (11 mM MGM) and hyperglycemia (25 mM HG).*

Fig. 14 shows the results for 7 analyzed masses included in the GSL group in relation to *β*-cells, large and small EVs Changes in this lipid group were observed both concerning culture conditions and sample type. For the cell, HG conditions caused a change in proportions, which means a significant increase in the content of $[C_{42}H_{81}NO_3Na]^+$ GSL molecular ion 18:0 with Na (*m/z* 750.49), $[C_{42}H_{81}NO_3Na]^+$ sulfatide 42:2 fragment (*m/z* 670, 47), $[C_{47}H_{91}NO_9Na]^+$ GSL molecular ion (*m/z* 836.80) with a decrease in the content for $[C_2H_9NPO_4]^+$ phosphosphingolipid fragment (*m/z* 142.07).

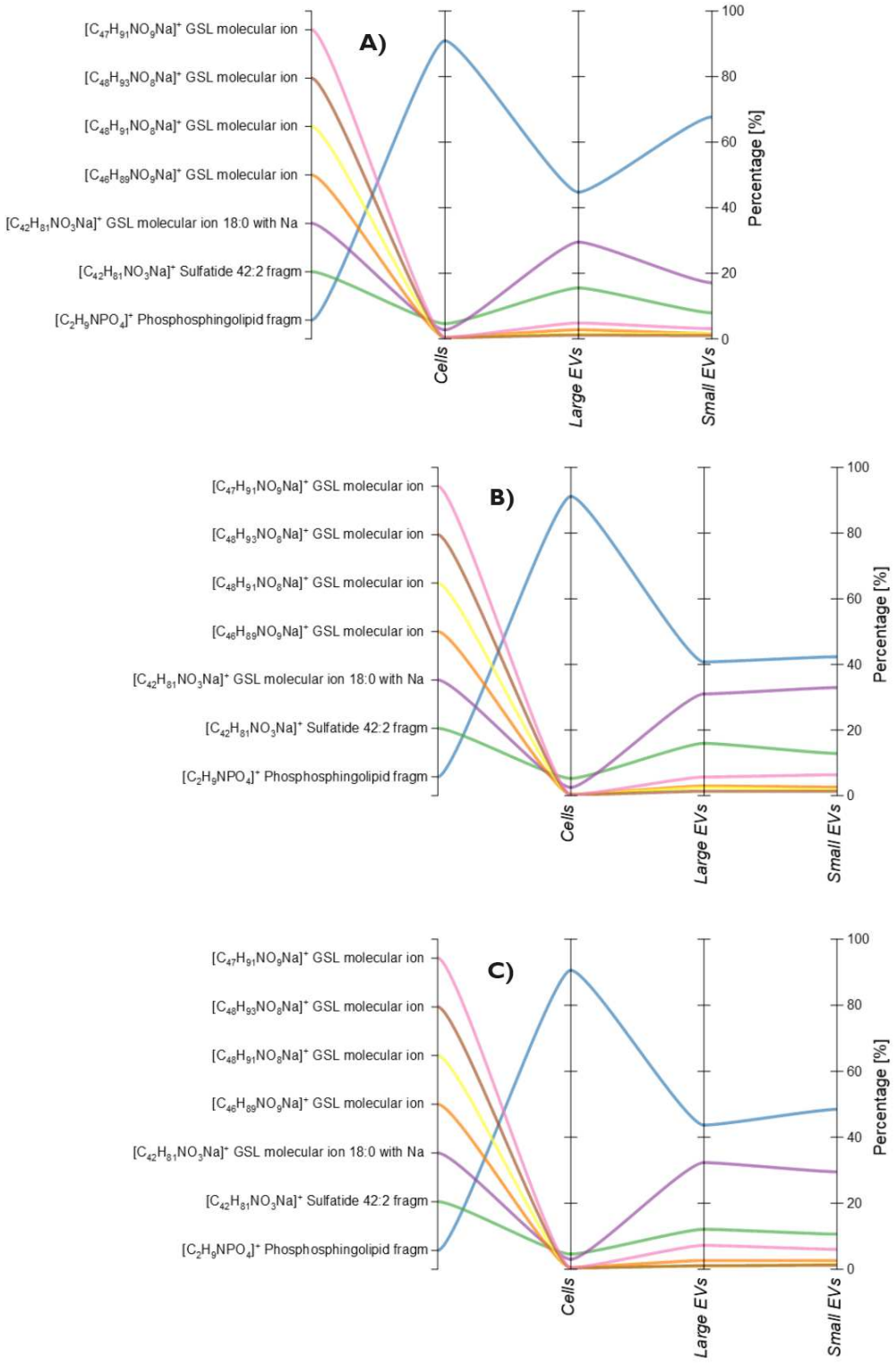

Fig. 15. *Percentage content changes in the case of the glycosphingolipids group for A) normoglycemic cells (5 mM D-glucose), B) moderately glycemic cells (11 mM glucose), C) hyperglycemic cells (25 mM D-glucose).*

Analyzing the results in terms of sample type (**Fig. 15**), it can be seen that there are no significant changes under NG conditions in the GLS ratio between cells, large and small EVs. For medium and high HG, an increase in the content of $[C_{47}H_{91}NO_9Na]^+$ GSL molecular ion (*m/z* 836.80) and $[C_{42}H_{81}NO_3Na]^+$ GSL molecular ion 18:0 with Na (*m/z* 750.49) in large and small ones is visible.

4. Discussion

HG is characterized by a condition in which there is too much sugar in the blood because the body does not have enough insulin for it to be absorbed and metabolized. It mainly affects people with diabetes and can have serious long-term consequences. Certainly, in the long run, the state of elevated glucose disturbs the sugar metabolism and changes the physiology of the biological system. Pancreatic β-cells are certainly such a biological system. These cells secrete EVs, which are undeniably transporters of information. The transfer of information takes place at many levels, an example is the change in the amount and presence of molecular compounds. An example of such compounds are SPs, which occur in cells, but also in EVs. CER, HexCER and GSLs are lipids included in the complexes responsible for molecular processes taking place inside the cell, and they can also be informative molecules reflecting changes in the amount and presence of the occurring pathological states. We speculate that this might be a signal in their presence about the changes resulting from HG. And so, the results show a significantly lower content of selected lipids from the listed classes due to the presence of hyperglycemia.

Earlier work showed that small EVs are enriched with specific lipids, i.e. glycosphingolipids, sphingomyelin, cholesterol and phosphatidylserine [24]. The comparative analysis carried out for this work confirmed that the small subpopulation of EVs is characterized by higher levels of mean, normalized intensity values in relation to the cells from which they originate. Moreover, the lipid profile depends both on the type of cell, and also on its physiological state, summing up the EVs from physiological cells may differ in composition from cells cultured in conditions of disturbed physiology, e.g. HG. There are also demonstrated differences in the composition of CER, HexCER and GSL between departmental subpopulations of EVs from a particular cell line [59]. Ceramide-containing lipids play many important roles in the human body and be involved in neurodegenerative diseases such as Alzheimer and Parkinson's. In this study, hyperglycemia and its effect on the level of ceramide-related lipids were taken into account [60,61]. The issue is important because it can be hypothesised that the principle of ceramide action on the content and

biogenesis of EVs in cells may have a similar effect of ceramides located on EVs. And just as EVs enriched with ceramides initiate apoptosis in astrocytes, a similar mechanism may occur in HG [62].

Further studies extending the known role of ceramides, hexceramides and glycosphingolipids in the development of pathological processes should be maintained using a novel approach. For this purpose, it is necessary to use new methods of identification and analysis.

5. Conclusions

In this study, the presence of both large and small EVs in isolated samples was confirmed not only through CryoTEM and TEM analyses but also via spectral flow cytometry, which is based on the detection of specific markers: CD9, CD63, CD81, and annexin-V. As demonstrated by Mathilde Mathieu et al., both tetraspanins CD9 and CD63 can be released in small ectosomes formed at the plasma membrane, a finding that our results corroborate [63]. Similar observations were reported in studies performed on the immortalized endothelial cells [16].

Utilizing ToF-SIMS mass spectrometry, we performed a comparative analysis of 38 lipids belonging to the sphingolipid group. In the analysis, mean, normalized intensity values from 12 individual spectra were compared for the experimental groups, β-cells from NG and HG, ectosomes from NG and HG, and exosomes from HG and NG. The examination of EVs content and distribution with ToF-SIMS can provide insight into the physiopathology associated with diabetes and contribute to the discovery of new biomarkers of early diagnosis and risk. While it has been shown that transported cargo EVs, such as mRNA and proteins, play a role, this work focuses on lipids and their informative function in communication *via* extracellular vesicles [64,65]. To the best of our knowledge, this is the first study to show TOF-SIMS results including a comparative analysis of ceramides, hexolysceramides and glycosphingolipids in extracellular vesicles derived from *β*-cells cultured in hyperglycemia.

Author contributions

M.S. – data curation, formal analysis, investigation, methodology, validation, visualisation, writing – original draft; M. D.-K. – investigation, methodology, validation, visualisation, writing original draft; E.Ł.S. conceptualization, formal analysis, funding acquisition, methodology, project administration, resources, supervision, writing – review & editing

Acknowledgements

1) This work was supported by the National Science Center (NCN), grant OPUS 17 to Prof. E. Stępień (No. 2019/33/B/NZ3/01004).

2) This work was supported by the ATOMIN 2.0 project (Grant Agreement No. 882117), funded by the under the Intelligent Development Operational Programme 2014-2020, Priority IV: Strengthening the research and development potential, Action 4.2: Development of modern research infrastructure of the science sector, Competition 4/4.2/2020. This funding enabled the purchase of state-of-the-art research equipment (ID7000 spectral flow cytometer, SONY).

3) This publication has been funded from the SciMat and qLife Priority Research Area budget under the Strategic Programme Excellence Initiative at the Jagiellonian University as the salary for M. D.-K.

4) This publication was developed under the provision of the Polish Ministry and Higher Education project Support for development research infrastructure of the National Synchrotron Radiation Centre SOLARIS under contract nr 1/SOL/2021/2.

5) The authors would like to thank Dr. Eng. Olga Woźnicka from the Institute of Zoology and Biomedical Research of the Jagiellonian University for providing TEM images. The authors would like to thank Dr. Michał Rawski from the National Synchroton Radiation Center SOLARIS Cryo-EM Facility for providing cryo-TEM images. The authors would like to thank Mrs Olena Bohomolova for her technical support during EVs isolation.

References:

[1] W. Zheng, J. Kollmeyer, H. Symolon, A. Momin, E. Munter, E. Wang, S. Kelly, J.C. Allegood, Y. Liu, Q. Peng, H. Ramaraju, M.C. Sullards, M. Cabot, A.H. Merrill, Ceramides and other bioactive sphingolipid backbones in health and disease: Lipidomic analysis, metabolism and roles in membrane structure, dynamics, signaling and autophagy, Biochimica et Biophysica Acta (BBA) - Biomembranes 1758 (2006) 1864–1884. https://doi.org/https://doi.org/10.1016/j.bbamem.2006.08.009.

[2] A.H. Merrill, T.H. Stokes, A. Momin, H. Park, B.J. Portz, S. Kelly, E. Wang, M.C. Sullards, M.D. Wang, Sphingolipidomics: a valuable tool for understanding the roles of sphingolipids in biology and disease, J Lipid Res 50 (2009) S97–S102. https://doi.org/10.1194/jlr.R800073-JLR200.

[3] E.Ł. Stępień, M. Durak-Kozica, P. Moskal, Extracellular vesicles in vascular pathophysiology: beyond their molecular content, Pol Arch Intern Med 133 (2023) 16483. https://doi.org/10.20452/pamw.16483.

[4] M.K. Cavaghan, D.A. Ehrmann, K.S. Polonsky, Interactions between insulin resistance and insulin secretion in the development of glucose intolerance., The Journal of Clinical Investigation 106 (2000) 329–333. https://doi.org/10.1172/JCI10761.

[5] M.E. Cerf, Beta cell dysfunction and insulin resistance., Frontiers in Endocrinology 4 (2013) 37. https://doi.org/10.3389/fendo.2013.00037.

[6] J.L. Leahy, Pathogenesis of Type 2 Diabetes Mellitus, Archives of Medical Research 36 (2005) 197–209. https://doi.org/https://doi.org/10.1016/j.arcmed.2005.01.003.

[7] M.T. Malecki, Type 2 diabetes mellitus and its complications: from the molecular biology to the clinical practice., The Review of Diabetic Studies : RDS 1 (2004) 5–8. https://doi.org/10.1900/RDS.2004.1.5.

[8] T. Tomita, Apoptosis in pancreatic β-islet cells in Type 2 diabetes., Bosnian Journal of Basic Medical Sciences 16 (2016) 162–179. https://doi.org/10.17305/bjbms.2016.919.

[9] Z. Fu, E.R. Gilbert, D. Liu, Regulation of insulin synthesis and secretion and pancreatic Beta-cell dysfunction in diabetes, Current Diabetes Reviews 9 (2013) 25–53.

[10] S.B. Russo, J.S. Ross, L.A. Cowart, Sphingolipids in obesity, type 2 diabetes, and metabolic disease., Handbook of Experimental Pharmacology (2013) 373–401. https://doi.org/10.1007/978-3-7091-1511-4_19.

[11] N. Tofte, T. Suvitaival, L. Ahonen, S.A. Winther, S. Theilade, M. Frimodt-Møller, T.S. Ahluwalia, P. Rossing, Lipidomic analysis reveals sphingomyelin and phosphatidylcholine species associated with renal impairment and all-cause mortality in type 1 diabetes, Scientific Reports 9 (2019) 16398. https://doi.org/10.1038/s41598-019-52916-w.

[12] M.E. Marzec, D. Wojtysiak, K. Połtowicz, J. Nowak, R. Pedrys, Study of cholesterol and vitamin E levels in broiler meat from different feeding regimens by TOF-SIMS, Biointerphases 11 (2016). https://doi.org/10.1116/1.4943619.

[13] D.C. Fernández-Remolar, D. Gómez-Ortiz, P. Malmberg, T. Huang, Y. Shen, A. Anglés, R. Amils, Preservation of Underground Microbial Diversity in Ancient Subsurface Deposits (>6 Ma) of

the Rio Tinto Basement, Microorganisms 9 (2021). https://doi.org/10.3390/microorganisms9081592.

[14] T.B. Angerer, D. Velickovic, C.D. Nicora, J.E. Kyle, D.J. Graham, C. Anderton, L.J. Gamble, Exploiting the Semidestructive Nature of Gas Cluster Ion Beam Time-of-Flight Secondary Ion Mass Spectrometry Imaging for Simultaneous Localization and Confident Lipid Annotations, Analytical Chemistry 91 (2019) 15073–15080. https://doi.org/10.1021/acs.analchem.9b03763.

[15] D.-K. Kim, J. Lee, S.R. Kim, D.-S. Choi, Y.J. Yoon, J.H. Kim, G. Go, D. Nhung, K. Hong, S.C. Jang, S.-H. Kim, K.-S. Park, O.Y. Kim, H.T. Park, J.H. Seo, E. Aikawa, M. Baj-Krzyworzeka, B.W.M. Van Balkom, M. Belting, L. Blanc, V. Bond, A. Bongiovanni, F.E. Borràs, L. Buée, E.I. Buzás, L. Cheng, A. Clayton, E. Cocucci, C.S. Dela Cruz, D.M. Desiderio, D. Di Vizio, K. Ekström, J.M. Falcon-Perez, C. Gardiner, B. Giebel, D.W. Greening, J. Christina Gross, D. Gupta, A. Hendrix, A.F. Hill, M.M. Hill, E. Nolte-'T Hoen, D.W. Hwang, J. Inal, M.V. Jagannadham, M. Jayachandran, Y.-K. Jee, M. Jørgensen, K.P. Kim, Y.-K. Kim, T. Kislinger, C. Lässer, D.S. Lee, H. Lee, J. Van Leeuwen, T. Lener, M.-L. Liu, J. Lötvall, A. Marcilla, S. Mathivanan, A. Möller, J. Morhayim, F. Mullier, I. Nazarenko, R. Nieuwland, D.N. Nunes, K. Pang, J. Park, T. Patel, G. Pocsfalvi, H. Del Portillo, U. Putz, M.I. Ramirez, M.L. Rodrigues, T.-Y. Roh, F. Royo, S. Sahoo, R. Schiffelers, S. Sharma, P. Siljander, R.J. Simpson, C. Soekmadji, P. Stahl, A. Stensballe, E. Stepień, H. Tahara, A. Trummer, H. Valadi, L.J. Vella, S.N. Wai, K. Witwer, M. Yánez-Mó, H. Youn, R. Zeidler, Y.S. Gho, EVpedia: A community web portal for extracellular vesicles research, Bioinformatics 31 (2015). https://doi.org/10.1093/bioinformatics/btu741.

[16] M. Durak-Kozica, A. Wróbel, M. Platt, E.Ł. Stępień, Comparison of qNANO results from the isolation of extracellular microvesicles with the theoretical model, Bio-Algorithms and Med-Systems 18 (2022) 171–179. https://doi.org/10.2478/bioal-2022-0088.

[17] K.W. Witwer, C. Théry, Extracellular vesicles or exosomes? On primacy, precision, and popularity influencing a choice of nomenclature, J Extracell Vesicles 8 (2019) 1648167. https://doi.org/10.1080/20013078.2019.1648167.

[18] E.Ł. St□pien, M. Durak-Kozica, A. Kamińska, M. Targosz-Korecka, M. Libera, G. Tylko, A. Opalińska, M. Kapusta, B. Solnica, A. Georgescu, M.C. Costa, A. Czyzewska-Buczyńska, W. Witkiewicz, M.T. Malecki, F.J. Enguita, Circulating ectosomes: Determination of angiogenic microRNAs in type 2 diabetes, Theranostics 8 (2018). https://doi.org/10.7150/thno.23334.

[19] M. Yáñez-Mó, P.R.-M. Siljander, Z. Andreu, A.B. Zavec, F.E. Borràs, E.I. Buzas, K. Buzas, E. Casal, F. Cappello, J. Carvalho, E. Colás, A. Cordeiro-da Silva, S. Fais, J.M. Falcon-Perez, I.M. Ghobrial, B. Giebel, M. Gimona, M. Graner, I. Gursel, M. Gursel, N.H.H. Heegaard, A. Hendrix, P. Kierulf, K. Kokubun, M. Kosanovic, V. Kralj-Iglic, E.-M. Krämer-Albers, S. Laitinen, C. Lässer, T. Lener, E. Ligeti, A. Linē, G. Lipps, A. Llorente, J. Lötvall, M. Manček-Keber, A. Marcilla, M. Mittelbrunn, I. Nazarenko, E.N.M. Nolte-'t Hoen, T.A. Nyman, L. O'Driscoll, M. Olivan, C. Oliveira, É. Pállinger, H.A. Del Portillo, J. Reventós, M. Rigau, E. Rohde, M. Sammar, F. Sánchez-Madrid, N. Santarém, K. Schallmoser, M.S. Ostenfeld, W. Stoorvogel, R. Stukelj, S.G. Van der Grein, M.H. Vasconcelos, M.H.M. Wauben, O. De Wever, Biological properties of extracellular vesicles and their physiological functions, Journal of Extracellular Vesicles 4 (2015) 27066. https://doi.org/10.3402/jev.v4.27066.

[20] M.A. Di Bella, Overview and Update on Extracellular Vesicles: Considerations on Exosomes and Their Application in Modern Medicine., Biology 11 (2022). https://doi.org/10.3390/biology11060804.

[21] E.Ł. Stępień, A. Kamińska, M. Surman, D. Karbowska, A. Wróbel, M. Przybyło, Fourier-Transform InfraRed (FT-IR) spectroscopy to show alterations in molecular composition of EV subpopulations from melanoma cell lines in different malignancy, Biochem Biophys Rep 25 (2021) 100888. https://doi.org/10.1016/j.bbrep.2020.100888.

[22] C. Rząca, U. Jankowska, E.Ł. Stępień, Proteomic profiling of exosomes derived from pancreatic beta-cells cultured under hyperglycemia, Bio-Algorithms and Med-Systems 18 (2022) 151–157. https://doi.org/doi:10.2478/bioal-2022-0085.

[23] E. St□pień, C. Rzaca, P. Moskal, Novel biomarker and drug delivery systems for theranostics - Extracellular vesicles, Bio-Algorithms and Med-Systems 17 (2021) 301–309. https://doi.org/10.1515/bams-2021-0183.

[24] A. Llorente, T. Skotland, T. Sylvänne, D. Kauhanen, T. Róg, A. Orłowski, I. Vattulainen, K. Ekroos, K. Sandvig, Molecular lipidomics of exosomes released by PC-3 prostate cancer cells, Biochimica et Biophysica Acta (BBA) - Molecular and Cell Biology of Lipids 1831 (2013) 1302–1309. https://doi.org/https://doi.org/10.1016/j.bbalip.2013.04.011.

[25] K. Carayon, K. Chaoui, E. Ronzier, I. Lazar, J. Bertrand-Michel, V. Roques, S. Balor, F. Terce, A. Lopez, L. Salomé, E. Joly, Proteolipidic Composition of Exosomes Changes during Reticulocyte Maturation, Journal of Biological Chemistry 286 (2011) 34426–34439. https://doi.org/10.1074/jbc.M111.257444.

[26] L. Musante, D. Tataruch, D. Gu, A. Benito-Martin, G. Calzaferri, S. Aherne, H. Holthofer, A Simplified Method to Recover Urinary Vesicles for Clinical Applications and Sample Banking, Scientific Reports 4 (2014) 7532. https://doi.org/10.1038/srep07532.

[27] A. Kamińska, M. Roman, A. Wróbel, A. Gala-Błądzińska, M.T. Małecki, C. Paluszkiewicz, E.Ł. Stępień, Raman spectroscopy of urinary extracellular vesicles to stratify patients with chronic kidney disease in type 2 diabetes, Nanomedicine: Nanotechnology, Biology and Medicine 39 (2022) 102468. https://doi.org/https://doi.org/10.1016/j.nano.2021.102468.

[28] M.E. Marzec, C. Rząca, P. Moskal, E. Stępień, Study of the influence of hyperglycemia on the abundance of amino acids, fatty acids, and selected lipids in extracellular vesicles using TOF-SIMS, Biochem Biophys Res Commun 622 (2022) 30–36. https://doi.org/10.1016/j.bbrc.2022.07.020.

[29] M.E. Marzec, D. Wojtysiak, K. Połtowicz, J. Nowak, R. Pedrys, Study of cholesterol and vitamin E levels in broiler meat from different feeding regimens by TOF-SIMS, Biointerphases 11 (2016) 02A326. https://doi.org/10.1116/1.4943619.

[30] A. Kamińska, M.E. Marzec, E.Ł. Stępień, Design and Optimization of a Biosensor Surface Functionalization to Effectively Capture Urinary Extracellular Vesicles., Molecules (Basel, Switzerland) 26 (2021). https://doi.org/10.3390/molecules26164764.

[31] D.J. Graham, D.G. Castner, Image and Spectral Processing for ToF-SIMS Analysis of Biological Materials., Mass Spectrometry (Tokyo, Japan) 2 (2013) S0014. https://doi.org/10.5702/massspectrometry.S0014.

[32] B.J. Tyler, G. Rayal, D.G. Castner, Multivariate analysis strategies for processing ToF-SIMS images of biomaterials, 28 (2007) 2412–2423. https://doi.org/10.1016/j.biomaterials.2007.02.002.

[33] M. Skalska, M. Durak-Kozica, Experimental and analytical procedures for ToF-SIMS measurement data of membranous structures., Bio-Algorithms and Med-Systems 19 (2023) 1–7.

[34] S. Hallal, Á. Tűzesi, G.E. Grau, M.E. Buckland, K.L. Alexander, Understanding the extracellular vesicle surface for clinical molecular biology., Journal of Extracellular Vesicles 11 (2022) e12260. https://doi.org/10.1002/jev2.12260.

[35] Y. Zhang, Y. Liu, H. Liu, W.H. Tang, Exosomes: biogenesis, biologic function and clinical potential, Cell & Bioscience 9 (2019) 19. https://doi.org/10.1186/s13578-019-0282-2.

[36] S. Keerthikumar, D. Chisanga, D. Ariyaratne, H. Al Saffar, S. Anand, K. Zhao, M. Samuel, M. Pathan, M. Jois, N. Chilamkurti, L. Gangoda, S. Mathivanan, ExoCarta: A Web-Based Compendium of Exosomal Cargo, J Mol Biol 428 (2016) 688–692. https://doi.org/10.1016/j.jmb.2015.09.019.

[37] B.M. Castro, M. Prieto, L.C. Silva, Ceramide: A simple sphingolipid with unique biophysical properties, Progress in Lipid Research 54 (2014) 53–67. https://doi.org/https://doi.org/10.1016/j.plipres.2014.01.004.

[38] T. Skotland, N.P. Hessvik, K. Sandvig, A. Llorente, Exosomal lipid composition and the role of ether lipids and phosphoinositides in exosome biology, Journal of Lipid Research 60 (2019) 9–18. https://doi.org/https://doi.org/10.1194/jlr.R084343.

[39] L. Salimi, A. Akbari, N. Jabbari, B. Mojarad, A. Vahhabi, S. Szafert, S.A. Kalashani, H. Soraya, M. Nawaz, J. Rezaie, Synergies in exosomes and autophagy pathways for cellular homeostasis and metastasis of tumor cells, Cell & Bioscience 10 (2020) 64. https://doi.org/10.1186/s13578-020-00426-y.

[40] M. Record, S. Silvente-Poirot, M. Poirot, M.J.O. Wakelam, Extracellular vesicles: Lipids as key components of their biogenesis and functions, Journal of Lipid Research 59 (2018) 1316–1324. https://doi.org/10.1194/jlr.E086173.

[41] T. Matsui, F. Osaki, S. Hiragi, Y. Sakamaki, M. Fukuda, ALIX and ceramide differentially control polarized small extracellular vesicle release from epithelial cells, EMBO Reports 22 (2021) e51475. https://doi.org/https://doi.org/10.15252/embr.202051475.

[42] G.O. Skryabin, A. V Komelkov, E.E. Savelyeva, E.M. Tchevkina, Lipid Rafts in Exosome Biogenesis, Biochemistry (Moscow) 85 (2020) 177–191. https://doi.org/10.1134/S0006297920020054.

[43] E. Bieberich, Sphingolipids and lipid rafts: Novel concepts and methods of analysis., Chemistry and Physics of Lipids 216 (2018) 114–131. https://doi.org/10.1016/j.chemphyslip.2018.08.003.

[44] P. Sigmund, Theory of Sputtering. I. Sputtering Yield of Amorphous and Polycrystalline Targets, Physical Review 184 (1969) 383–416.

[45] C.C. Geilen, T. Wieder, C.E. Orfanos, Ceramide signalling: regulatory role in cell proliferation, differentiation and apoptosis in human epidermis., Archives of Dermatological Research 289 (1997) 559–566. https://doi.org/10.1007/s004030050240.

[46] O. Quehenberger, A.M. Armando, A.H. Brown, S.B. Milne, D.S. Myers, A.H. Merrill, S. Bandyopadhyay, K.N. Jones, S. Kelly, R.L. Shaner, C.M. Sullards, E. Wang, R.C. Murphy, R.M. Barkley, T.J. Leiker, C.R.H. Raetz, Z. Guan, G.M. Laird, D.A. Six, D.W. Russell, J.G. McDonald, S. Subramaniam, E. Fahy, E.A. Dennis, Lipidomics reveals a remarkable diversity of lipids in human plasma1[S], Journal of Lipid Research 51 (2010) 3299–3305. https://doi.org/https://doi.org/10.1194/jlr.M009449.

[47] B.W.S. Lam, T.Y.A. Yam, C.P. Chen, M.K.P. Lai, W.-Y. Ong, D.R. Herr, The noncanonical chronicles: Emerging roles of sphingolipid structural variants, Cellular Signalling 79 (2021) 109890. https://doi.org/https://doi.org/10.1016/j.cellsig.2020.109890.

[48] U. Loizides-Mangold, F.P.A. David, V.J. Nesatyy, T. Kinoshita, H. Riezman, Glycosylphosphatidylinositol anchors regulate glycosphingolipid levels., Journal of Lipid Research 53 (2012) 1522–1534. https://doi.org/10.1194/jlr.M025692.

[49] S. Hakomori, Carbohydrate-to-carbohydrate interaction in basic cell biology: a brief overview., Archives of Biochemistry and Biophysics 426 (2004) 173–181. https://doi.org/10.1016/j.abb.2004.02.032.

[50] A. Regina Todeschini, S. Hakomori, Functional role of glycosphingolipids and gangliosides in control of cell adhesion, motility, and growth, through glycosynaptic microdomains., Biochimica et Biophysica Acta 1780 (2008) 421–433. https://doi.org/10.1016/j.bbagen.2007.10.008.

[51] S. Sonnino, L. Mauri, V. Chigorno, A. Prinetti, Gangliosides as components of lipid membrane domains, Glycobiology 17 (2007) 1R-13R. https://doi.org/10.1093/glycob/cwl052.

[52] G. Gupta, A. Surolia, Glycosphingolipids in microdomain formation and their spatial organization., FEBS Letters 584 (2010) 1634–1641. https://doi.org/10.1016/j.febslet.2009.11.070.

[53] N.M. Hooper, Detergent-insoluble glycosphingolipid/cholesterol-rich membrane domains, lipid rafts and caveolae (review)., Molecular Membrane Biology 16 (1999) 145–156. https://doi.org/10.1080/096876899294607.

[54] C.A. Lingwood, Glycosphingolipid functions., Cold Spring Harbor Perspectives in Biology 3 (2011). https://doi.org/10.1101/cshperspect.a004788.

[55] G. D'Angelo, S. Capasso, L. Sticco, D. Russo, Glycosphingolipids: synthesis and functions., The FEBS Journal 280 (2013) 6338–6353. https://doi.org/10.1111/febs.12559.

[56] Z. Vukelić, S. Kalanj-Bognar, M. Froesch, L. Bîndila, B. Radić, M. Allen, J. Peter-Katalinić, A.D. Zamfir, Human gliosarcoma-associated ganglioside composition is complex and distinctive as evidenced by high-performance mass spectrometric determination and structural characterization., Glycobiology 17 (2007) 504–515. https://doi.org/10.1093/glycob/cwm012.

[57] D.D. Park, G. Xu, M. Wong, C. Phoomak, M. Liu, N.E. Haigh, S. Wongkham, P. Yang, E. Maverakis, C.B. Lebrilla, Membrane glycomics reveal heterogeneity and quantitative

distribution of cell surface sialylation., Chemical Science 9 (2018) 6271–6285. https://doi.org/10.1039/c8sc01875h.

[58] G. van Echten-Deckert, J. Walter, Sphingolipids: critical players in Alzheimer's disease., Progress in Lipid Research 51 (2012) 378–393. https://doi.org/10.1016/j.plipres.2012.07.001.

[59] J.F. Brouwers, M. Aalberts, J.W.A. Jansen, G. van Niel, M.H. Wauben, T.A.E. Stout, J.B. Helms, W. Stoorvogel, Distinct lipid compositions of two types of human prostasomes, PROTEOMICS 13 (2013) 1660–1666. https://doi.org/https://doi.org/10.1002/pmic.201200348.

[60] N. Bengoa-Vergniory, R.F. Roberts, R. Wade-Martins, J. Alegre-Abarrategui, Alpha-synuclein oligomers: a new hope, Acta Neuropathologica 134 (2017) 819–838. https://doi.org/10.1007/s00401-017-1755-1.

[61] M.B. Dinkins, G. Wang, E. Bieberich, Sphingolipid-Enriched Extracellular Vesicles and Alzheimer's Disease: A Decade of Research, Journal of Alzheimer's Disease 60 (2017) 757–768. https://doi.org/10.3233/JAD-160567.

[62] G. Wang, M. Dinkins, Q. He, G. Zhu, C. Poirier, A. Campbell, M. Mayer-Proschel, E. Bieberich, Astrocytes Secrete Exosomes Enriched with Proapoptotic Ceramide and Prostate Apoptosis Response 4 (PAR-4): POTENTIAL MECHANISM OF APOPTOSIS INDUCTION IN ALZHEIMER DISEASE (AD)*, Journal of Biological Chemistry 287 (2012) 21384–21395. https://doi.org/https://doi.org/10.1074/jbc.M112.340513.

[63] M. Mathieu, N. Névo, M. Jouve, J.I. Valenzuela, M. Maurin, F.J. Verweij, R. Palmulli, D. Lankar, F. Dingli, D. Loew, E. Rubinstein, G. Boncompain, F. Perez, C. Théry, Specificities of exosome versus small ectosome secretion revealed by live intracellular tracking of CD63 and CD9., Nature Communications 12 (2021) 4389. https://doi.org/10.1038/s41467-021-24384-2.

[64] G.E. Grieco, D. Fignani, C. Formichi, L. Nigi, G. Licata, C. Maccora, N. Brusco, G. Sebastiani, F. Dotta, Extracellular Vesicles in Immune System Regulation and Type 1 Diabetes: Cell-to-Cell Communication Mediators, Disease Biomarkers, and Promising Therapeutic Tools , Frontiers in Immunology 12 (2021).

[65] K.R. Giri, L. de Beaurepaire, D. Jegou, M. Lavy, M. Mosser, A. Dupont, R. Fleurisson, L. Dubreil, M. Collot, P. Van Endert, J.-M. Bach, G. Mignot, S. Bosch, Molecular and Functional Diversity of Distinct Subpopulations of the Stressed Insulin-Secreting Cell's Vesiculome , Frontiers in Immunology 11 (2020).

Supplementary A

Ceramides

Mass [m/z]	*Formula of ion*	*Indeks*
510,35	$[C_{32}H_{63}NO_3]^+$ Cer 32:1	**1**
508,31	$[C_{32}H_{61}NO_3]^+$ Cer 32:2	**2**
538,59	$[C_{34}H_{67}NO_3]^+$ Cer 34:1	**3**
536,60	$[C_{34}H_{65}NO_3]^+$ Cer 34:2	**4**
568,37	$[C_{36}H_{73}NO_3]^+$ Cer 36:0	**5**
566,35	$[C_{36}H_{71}NO_3]^+$ Cer 36:1	**6**
592,37	$[C_{38}H_{73}NO_3]^+$ Cer 38:2	**7**
620,60	$[C_{40}H_{77}NO_3]^+$ Cer 40:2	**8**
622,33	$[C_{40}H_{79}NO_3]^+$ Cer 40:1	**9**
632,64	$[C_{41}H_{77}NO_3]^+$ Cer 41:3	**10**
636,65	$[C_{41}H_{81}NO_3]^+$ Cer 41:1	**11**
650,65	$[C_{42}H_{83}NO_3]^+$ Cer 42:1	**12**

HexCeramides

Mass [m/z]	*Formula of ion*	*Indeks*
702,37	$[C_{40}H_{79}NO_8]^+$ HexCer 34:0	**1**
700,35	$[C_{40}H_{77}NO_8]^+$ HexCer 34:1	**2**
698,35	$[C_{40}H_{75}NO_8]^+$ HexCer 34:2	**3**
730,29	$[C_{42}H_{83}NO_8]^+$ HexCer 36:0	**4**
728,61	$[C_{42}H_{81}NO_8]^+$ HexCer 36:1	**5**
726,44	$[C_{42}H_{79}NO_8]^+$ HexCer 36:2	**6**
760,47	$[C_{44}H_{89}NO_8]^+$ HexCer 38:0	**7**
756,37	$[C_{44}H_{85}NO_8]^+$ HexCer 38:1	**8**
754,29	$[C_{44}H_{83}NO_8]^+$ HexCer 38:2	**9**
786,45	$[C_{46}H_{91}NO_8]^+$ HexCer 40:0	**10**
784,29	$[C_{46}H_{89}NO_8]^+$ HexCer 40:1	**11**
782,28	$[C_{46}H_{87}NO_8]^+$ HexCer 40:2	**12**
798,39	$[C_{47}H_{91}NO_8]^+$ HexCer 41:1	**13**

814,45	$[C_{48}H_{95}NO_8]^+$ HexCer 42:0	**14**
812,46	$[C_{48}H_{93}NO_8]^+$ HexCer 42:1	**15**
810,41	$[C_{48}H_{91}NO_8]^+$ HexCer 42:2	**16**
808,37	$[C_{48}H_{89}NO_8]^+$ HexCer 42:3	**17**

Glycosphingolipids

Mass [m/z]	***Formula of ion***	***Indeks***
86,10	$[C_5H_{12}N]^+$ Sfingocholin fragm.	**1**
102,10	$[C_5H_{12}NO]^+$ Cer fragm.	**2**
104,11	$[C_5H_{14}NO]^+$ Cer fragm.	**3**
142,03	$[C_2H_9NPO_4]^+$ GSL fragm.	**4**
184,09	$[C_5H_{14}NO]^+$ Cer fragm.	**5**
282,32	$[C_{18}H_{34}O_2]^+$ Cer 36:1 fragm.	**6**
670,38	$[C_{42}H_{81}NO_3Na]^+$ Sulfatide 42:2	**7**
750,35	$[C_{42}H_{81}NO_3Na]^+$ GSL mol. ion	**8**
822,53	$[C_{46}H_{89}NO_9Na]^+$ GSL mol. ion	**9**
832,60	$[C_{48}H_{91}NO_8Na]^+$ GSL mol. ion	**10**
834,64	$[C_{48}H_{93}NO_8Na]^+$ GSL mol. ion	**11**
836,67	$[C_{47}H_{91}NO_9Na]^+$ GSL mol. ion	**12**